Raindrop Size Distribution and Rainfall Attenuation Modeling from Disdrometer Measurement in Central Africa: Case of Cameroon

Patrick H. Ntanguen[1, 2, *], Armand Nzeukou[2], and Alain T. Sandjon[2]

Abstract—Raindrop sizes were measured in Douala, Cameroon ($4°03'$N, $9°42'$E) using a Parsivel[2] disdrometer. The data obtained are used for the analysis of the drop size distribution (DSD) and specific rain attenuation modeling in the 5–150 GHz frequency range. The Lognormal and gamma distribution models are employed using the method of moments estimation, considering the third, fourth, and sixth-order moments. The parameter fits for the two DSD models proposed here for different values of rain rates are investigated. The specific rainfall attenuation using the Douala DSD models is compared to the ITU-R models in vertical and horizontal polarization and models for some countries with different climates such as semi-arid, tropical, and subtropical ones in Africa. The comparison with the ITU-R model shows significant differences occurring at high frequency with both high and low rainfall rates. The comparison with other regions of Africa also shows that Douala is characterized by equatorial climate, and Durban characterized by subtropical climate shows similar rainfall attenuation characteristics at operating frequency range $10 \leq f \leq 150$ GHz, especially at a lower rain rate. At a higher rain rate, specific rain attenuation at Douala is always higher than in other African locations. The proposed models are very important for the determination of rainfall attenuation for terrestrial and satellite systems.

1. INTRODUCTION

Attenuation of millimetre waves is regularly caused by hydrometeors (Snow, Hail, Rain, etc.), but among them, the most severe one is that caused by rain [1]. In radiocommunication, rain attenuation is also one of the limiting factors for frequency bands above 10 GHz [2], because in these frequency bands, the propagation wavelength is comparable to the size of the rain droplet [3]. For the prediction of rain attenuation, the most important parameters are raindrop size distribution (DSD) and the rainfall rate [4, 5]. However, a lot of works have already been done on the measurement of raindrop size distribution, rain rate, and radar reflectivity to study the attenuation observed on radio signals caused by microwave and millimetre waves. In order to have a mastery on the attenuation due to rain caused by microwaves and millimetre waves, many works have already been carried out on the measurement of raindrops size distribution [6]. Studies carried out in temperate regions have shown very good results in terms of the attenuation resulting from the rains, which is made possible by the availability of data recorded in these regions. Compared to tropical regions and more precisely to Africa, there is a lack of data availability due to the lack of finances to purchase the necessary equipment to make the measurements which is very expensive. Nevertheless, some countries in Africa have been able to accumulate a lot of data on raindrops and have used these data to develop distribution models and test the fit of these models on the data, as presented by Ojo et al. in Nigeria [7], Ochou et al. in Niger, Ivory

[1] Research Unit Condensed Matter, Electronics and Signal Processing, Department of Physics, University of Dschang, Cameroon.
[2] Unité de Recherche d'ingenierie des Systèmes Industriels et de l'environnement (UR-ISIE), Institut Universitaire de Technologie Fotso Victor, Université de Dschang, Cameroon.

Coast, and Senegal [8], Sumbiri and Adetan in Rwanda [6, 10], and Alonge et Afullo in South Africa [9]. Works were carried out in different climatic zones, namely tropical, subtropical, and semi-arid regions.

The purpose of this work is to analyse the raindrop size distribution in the Central African area and more specifically in Douala-Cameroon (4°03′N, 9°42′E) using the lognormal and gamma distribution models, to apply these two models of distribution in the determination of the specific rain attenuation using the Mie Scattering theory and the temperature of 25°C for spherical raindrop shape, and finally to make a comparative study between the results obtained in this work and those of the other regions of Africa presented above.

2. MATERIALS AND METHODS

2.1. Data Collection

The rainfall data were measured using the second generation OTT Parsivel² disdrometer [12], manufactured by the German company Messtechnik. The disdrometer is installed in a well-appointed space in the courtyard of the University Institute of Technology of Douala (UIT) in Cameroon (4° 03′N, 9° 42′E at 13 m a.s.l) over 07 months between March and September 2019. It consists of an optical sensor emitting a 1 mm thick laser light beam with a horizontal area of $180 \times 30 \, \text{mm}^2$ 54 cm²) and a wavelength of 780 nm. The disdrometer can measure sizes up to 24.5 mm and uses 32 bins of various widths, ranging from 0.125 to 3 mm. The smallest and largest detectable drop velocity is about 0.05 m/s and 20.8 m/s, respectively. The velocity is subdividing into 32 bins with different widths, ranging from 0.1 to 3.2 m/s. The device provides a matrix with the number of drops recorded according to classes of equivolumic diameter and terminal fall velocity. With this matrix, it is possible to compute the rain rate R in mm · h⁻¹ (by counting the number of drops that fell during a time interval); and a drop size distribution (DSD) denoted $N(D)$ (m⁻³ mm⁻¹). The number concentration of raindrops per unit volume per unit size interval at the discrete instant has been calculated from the Parsivel² disdrometer is counted by the following.

$$N(D_i) = \frac{1}{S_{eff}(D_i)\Delta D_i \Delta t} \sum_{j=1}^{32} \frac{n_{i,j}}{v_j} \ \left(\text{m}^{-3}\,\text{mm}^{-1}\right) \tag{1}$$

where $n_{i,j}$ is the number of drops within the size bin i and velocity bin j; D_i (mm) is the raindrop diameter for the size bin i; ΔD_i is the corresponding diameter interval (mm); $v_j(ms^{-1})$ is the fall speed for the velocity bin j; $\Delta t(s)$ is the time; and $S_{eff}(m^2)$ is the sampling area of the device. In the data presented in the paper, S_{eff} is slightly modified according to the drop size to account for edge effects for large drops. For Parsivel², S_{eff} is expressed as $S_{eff}(D_i) = L(W - \frac{D_i}{2})$ where L and W are respectively the length and width of the sampling area [13, 14]. The rainfall rate (mm/h) for each time step is expressed as:

$$R = \frac{\pi}{6\Delta t} \sum_{j=1}^{32} \sum_{i=1}^{32} \frac{n_{i,j} D_j^3}{S_{eff}(D_i)} \tag{2}$$

for the dataset that the measuring time step is equal to 5 min.

For the data recorded by the Parsivel² in this paper, a filter method is included as suggested by various authors [13, 15, 16] to remove drops that, according to their size and velocity, are considered to be non-meteorological measurements. Practically, hydrometeors whose velocity differs more than 60% from the terminal fall velocity expected from its diameter and Beard's formula are removed [17].

In the entire period of measurement, 10935 rainfall samples had been recorded from the disdrometer for 7 months. The maximum number of raindrops per sample in the measurement period is 999 drops with a maximum rainfall rate of 128.8094 mm/h and a minimum of 0.0846 mm/h.

2.2. DSD Modeling

The distribution models regularly used are generally the gamma, lognormal, and exponential models. Gamma distribution is with 3 parameters which include scaling parameter (N_0), slope (Λ), and shape(μ).

At the same time, exponential distribution is with parameters which include intercept (N_0) and slope (Λ), respectively. Therefore in the present work, the lognormal and gamma models are taken into consideration to describe DSD characteristics.

The lognormal distribution model is given as follows [18–22].

$$N(D) = \frac{N_T \exp[-\ln^2(D/D_g)/2\ln^2 \sigma_g]}{\sqrt{2\pi}\ln(\sigma_g)D} \tag{3}$$

where $N(D)$ is considered as the number density (in $\mathrm{mm}^{-3}\,\mathrm{mm}^{-1}$), N_T as the total number of drops, D as the drop diameter (in mm), σ_g as the standard geometrical deviation of D, and D_g as the mean geometrical diameter of D.

The Gamma distribution model is given as follows [23, 24].

$$N(D) = N_0 D^\mu \exp(-\Lambda D) \tag{4}$$

where D (mm), $N(D)$ ($\mathrm{m}^{-3}\,\mathrm{mm}^{-1}$), N_0 ($\mathrm{mm}^{-1-\mu}\,\mathrm{m}^{-3}$), μ, and Λ (mm^{-1}) are the drop diameter, the number of drops per unit volume size interval, the intercept parameter, the shape parameter, and the slop parameter, respectively. To estimate their corresponding fit parameters, the moment method technique (MoM) is used with the third, fourth, and sixth moments of the observed spectra, as in [25].

The statistical moment at the nth order moment is expressed as [11, 26].

$$M_n = \sum_{i=1}^{N} D_i^n N(D_i)\Delta D_i \tag{5}$$

where $N(D_i)$ is the drop size distribution, ΔD_i the diameter interval, D_i the mean drop diameter in the ith class, and N the sample size.

The parameters for both rainfall DSD model are related to rain rate by the expressions (6) and (7) as:

For Gamma model:

$$\begin{cases} N_0 = A_0 R^{b_0} \\ \Lambda = A_\Lambda R^{b_\Lambda} \end{cases} \tag{6}$$
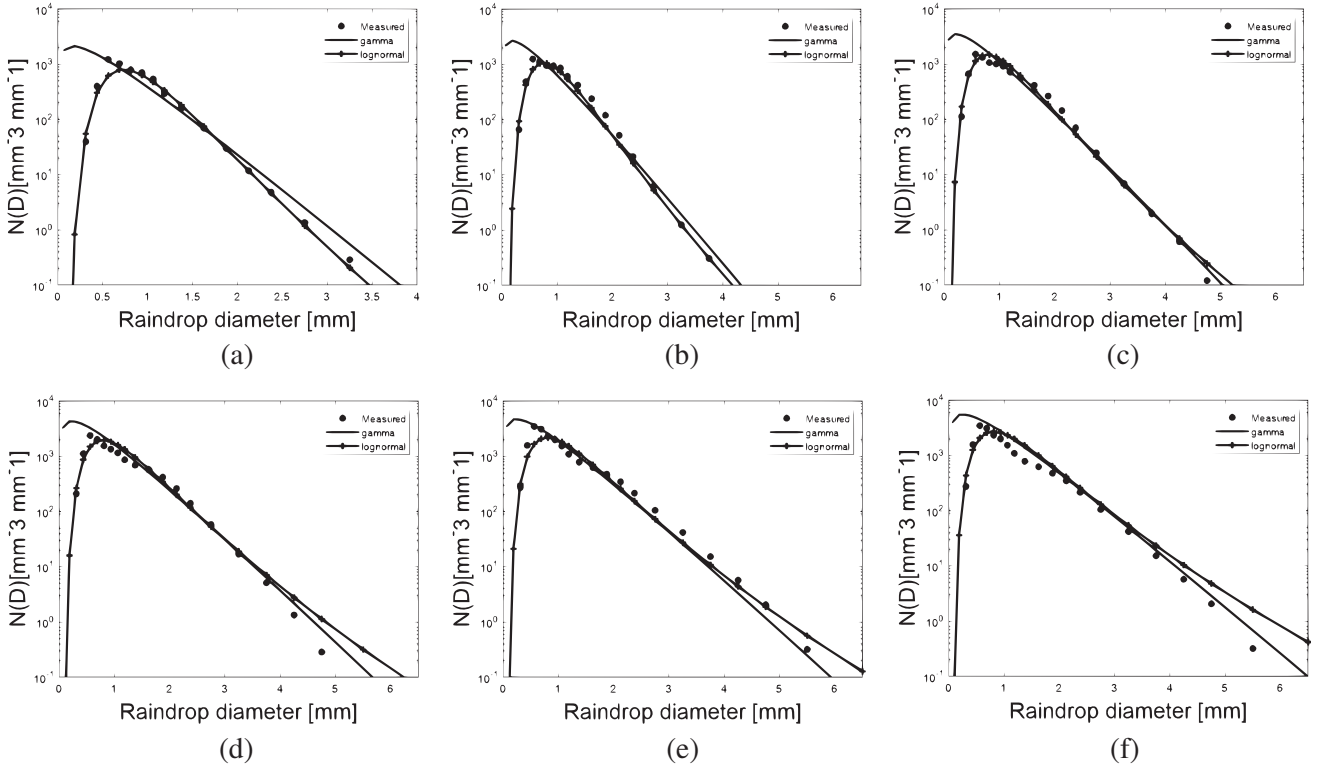
Lognormal Model:

$$\begin{cases} N_T = A_T R^{b_T} \\ D_g = A_{D_g} R^{b_{D_g}} \\ \sigma_g = A_{\sigma_g} R^{b_{\sigma_g}} \end{cases} \tag{7}$$

Here, A_0, b_0, A_Λ, b_Λ, A_T, b_T, A_{D_g}, b_{D_g}, A_{σ_g}, and b_{σ_g} are parameters of the model and evaluated by the least-squares method, and results are shown in Table 1.

Table 1. Model parameters for different rainfall DSD statistical models analysis in Douala, Cameroon.

Lognormal DSD model		
$N_T = A_T R^{b_T}$	$D_g = A_{D_g} R^{b_{D_g}}$	$\sigma_g = A_{\sigma_g} R^{b_{\sigma_g}}$
$240.97R^{0.543}$	$0.748R^{0.069}$	$1.349R^{0.042}$
Gamma DSD model		
μ	$N_0 = A_0 R^{b_0}$	$\Lambda = A_\Lambda R^{b_\Lambda}$
0.525	$6446R^{0.231}$	$4.039R^{-0.147}$

Using the estimated parameters in Table 1, lognormal and gamma DSD models for Douala are developed, and results are presented in Figs. 1(a)–1(f) at rainfall rates of 5 mm/h, 10 mm/h, 25 mm/h, 50 mm/h, 65 mm/h, and 110 mm/h, respectively.

Figure 1. Measured and fitted lognormal and gamma Rainfall drop size distribution models at (a) 5 mm/h, (b) 10.5 mm/h, (c) 25 mm/h, (d) 50 mm/h, (e) 65 mm/h, (f) 110 mm/h.

Table 2. RMSE for Lognormal and Gamma.

Rain Rates (mm/h)	RMSE	
	Lognormal	Gamma
1.54	0.334	1.248
9.25	1.371	9.628
21.35	2.729	23.488
60.25	37.225	120.943

2.3. Specific Rain Attenuation Modeling

The specific rainfall attenuation (attenuation per unit length over a fixed radio link) is a fundamental quantity in the calculation of the attenuation due to rain statistics for both terrestrial and earth-space paths [6, 27]. The specific attenuation coefficient due to rain using the DSD in decibels per kilometer can be computed by integrating each raindrop contribution as given by [6, 20, 28, 29, 30]:

$$A\,[\mathrm{dB/km}] = 4.343 \times 10^{-3} \int_0^\infty Q_{ext} N(D) dD \tag{8}$$

where A in (dB/km) is the specific rain attenuation; $N(D)$ is the drop size distribution in this study the lognormal and gamma DSD models are used; and Q_{ext} is the extinction cross-section of water spheres in mm^2 which is a function of the drop diameter D, the wavelength λ, and the complex refraction index of water m. The refractive index of the raindrop also depends on the propagating frequency, temperature,

and drop size distribution. Q_{ext} is given as:

$$Q_{ext}(D, \lambda, m) = \frac{\lambda^2}{2\pi} R_e \sum_{n=1}^{\infty} (2n+1)(a_n + b_n) \tag{9}$$

where a_n and b_n are the Mie scattering coefficients which depend on the drop diameter, wavelength, and complex refraction index of raindrops, and R_e is the real part of the forward scattering amplitude for spherical raindrops, which is the greater portion of the extinction cross-section coefficient. To determine the complex refractive index of the water, we used the model proposed by Liebe et al. [31]. The temperature of the rainy medium is considered 20°C in the ITU-R model (based on Laws-Parsons DSD), which is suitable for the temperate region [32]. Here, the temperature of the medium is considered to be 25°C.

Rainfall attenuation can also be estimated in the function of rainfall rate as proposed by Olsen et al. [33].

$$A\,(\mathrm{dB/km}) = kR^\alpha \tag{10}$$

where k and α are regression parameters that depend on many factors such as temperature, drop size distributions (DSD), and operating frequency. In Table 3, the values obtained for k and α are given.

Table 3. Coefficients for specific attenuation calculation form Lognormal and Gamma models.

Frequency (GHz)	Lognormal model		Gamma model	
	k	α	k	α
10	0.009	0.898	0.011	0.840
20	0.072	0.838	0.077	0.814
30	0.210	0.779	0.207	0.777
40	0.415	0.742	0.398	0.750
50	0.701	0.705	0.655	0.722
60	1.059	0.667	0.966	0.694
70	1.455	0.632	1.314	0.669
80	1.848	0.604	1.680	0.646
90	2.201	0.582	2.049	0.627
100	2.494	0.566	2.409	0.610

In the computation of the specific attenuation due to rain in Douala, Equation (10) has been used, and this estimation is based on the two raindrop size distribution models developed in section two.

3. RESULTS AND DISCUSSION

3.1. Variability of DSD Models in Douala

The characteristics of the lognormal and gamma DSD model parameters are given in Table 1. The models are estimated without any classification of rain, and they essentially represent the average characteristics of rainfall. It should be noted that these parameters are functions of rain rate, and the value of μ for the gamma model is taken to be 0.525 at this location. In Figs. 1(a)–1(f), modeled drop size distributions for two different DSD models with rain rates 5, 10.5, 25, 50, 65, and 110 mm/h, respectively, are shown. As demonstrated by Adetan and Afullo [34], an intrinsic change in the shapes of the DSD is observed as the rain rate increases.

In Fig. 1(a), for a rainfall rate of 5 mm/h, the lognormal model seems to coincide with the measured DSDs in all drop diameter regions, but there is a slight underestimation of the DSDs measured between 0.437 mm and 0.687 mm. The gamma model underestimates the measurement at the lower raindrop diameter region and overestimates for the larger raindrop diameter region. The lognormal DSD model fits the measured DSD better than the gamma model.

In Fig. 1(b), at a rainfall rate of 10.5 mm/h, the gamma model overestimates the measurement data for the lower raindrop diameter region, between 0.312 and 0.687 mm, and also for the larger raindrop diameter region from 2.125 mm. The lognormal model fits the measurement well at drop diameter region between 0.562 and 3.75 mm. For Figs. 1(a)–1(f), the lognormal model is found to fit better than the gamma model, but as the rain rate increases the lognormal model is found to have a poor fit for the large raindrop diameter regions. From the plotted graphs of Fig. 1, it is observed that the models perform differently as the rainfall rate changes. Therefore, there is a need for proper error estimation between the distribution models and the measured DSD at various rainfall rates to establish the best model in the region. For this purpose, the various DSD models were tested using the root mean square error (RMSE) test given by [35, 36]:

Using Equation (11), the results of the error estimation for different rainfall DSD models for Douala based on the four rainfall regimes are presented in Table 2. From Table 2, the DSD model giving the lowest RMSE will be the best fit to the measurements; therefore, by combining the information from Fig. 1 and Table 2, the Lognormal model best fits the measured data.

$$RMSE = \sqrt{\frac{\sum_{i=1}^{N} [N_{obs}(D_i) - N_{fit}(D_i)]^2}{N}} \tag{11}$$

where $N_{obs}(D_i)$ is the observed DSD at raindrop diameter D_i, $N_{fit}(D_i)$ the matched DSD at raindrop diameter D_i, and N the number of drop diameter bins of the DSD.

3.2. Variability of Specific Attenuation Distribution

Figure 2 shows the specific attenuation values with the two DSD models provided in Table 1 over the frequencies from 1 GHz to 120 GHz at four rain rates of 5, 10, 30, and 80 mm/h. These plots show comparisons between the specific rain attenuation for four rain rates using various DSD models, including the ITU-R estimate by horizontal and vertical polarizations [6, 37].

It can be seen from Fig. 2 that the specific attenuation due to rain increases as the frequency and rain rate increase. In Fig. 2(a), for rain rate at 5 mm/h, the ITU-R models (horizontal and vertical polarization) overestimate for frequencies less than 10 GHz, and overestimate between 10 and 50 GHz while they underestimate beyond this frequency.

For the 10 mm/h rainfall rate shown in Fig. 2(b), it can be seen that the ITU-R, Lognormal, and Gamma models match for frequencies up to 5 GHz, while the ITU-R models underestimate for the frequency range 5–60 GHz and overestimate for frequencies above 60 GHz. It is also observed from Fig. 2(c) and Fig. 2(d) that the ITU-R models underestimate for frequencies less than 10 GHz while overestimating for the measurement for frequencies above 60 GHz. It is also observed that the Lognormal model underestimates the specific attenuation for low frequency (0–60 GHz) compared to the gamma model, which overestimates for high frequency (above 60 GHz). The observed difference between the increase in attenuation values generated by the local DSD (lognormal and gamma models) and that of the ITU-R models when rain rates increase indicates a mismatch between the observed DSD and the Laws-Person DSD model.

3.3. Comparison with Other Measurement Sites in Africa

Figure 3(a) to Fig. 3(d) compare the specific attenuation (A) plots for the littoral coast of Cameroon with those of lognormal distribution for other tropical regions namely Boyélé, Republic of Congo (2°50′N, 18°04′E), Abidjan, Ivory Coast (5°25′N, 4°W), Butare, Rwanda (2°36′S, 29°44′E), and Ile-Ife, Nigeria (7°30′N, 4°30′E), for subtropical regions, namely, Durban, South Africa (29°52′S, 30°58′E) and semi-arid regions, namely, Dakar, Senegal (22°34′N, 17°29′W), and Niamey, Niger (13°30′N, 2°10′E). The lognormal distributions used in this comparison are the ones obtained by Alonge [21], and the corresponding parameters are shown in Table 4. The ambient (annual) temperature presented by Alonge [21] is assigned for each location as follows: Niamey (30°C), Abidjan, Boyélé, Dakar, and Ile-Ife (27°C), Durban and Butare (21°C), and Douala (25°C). The behavior and performance of specific
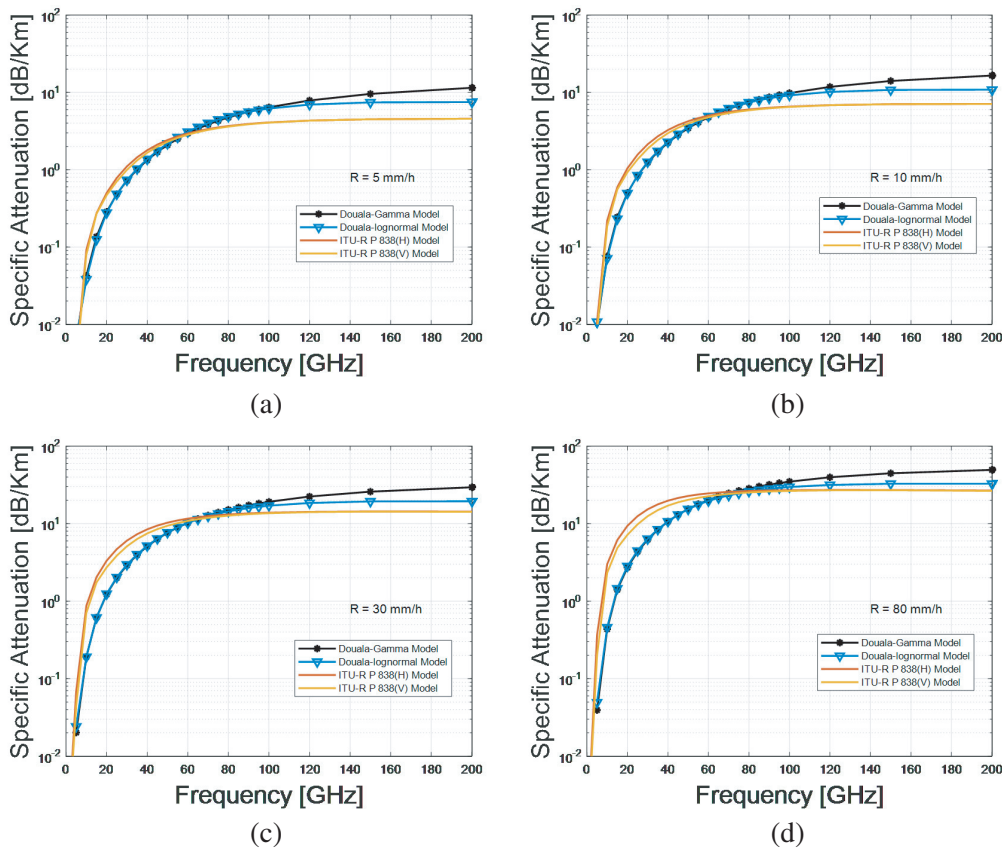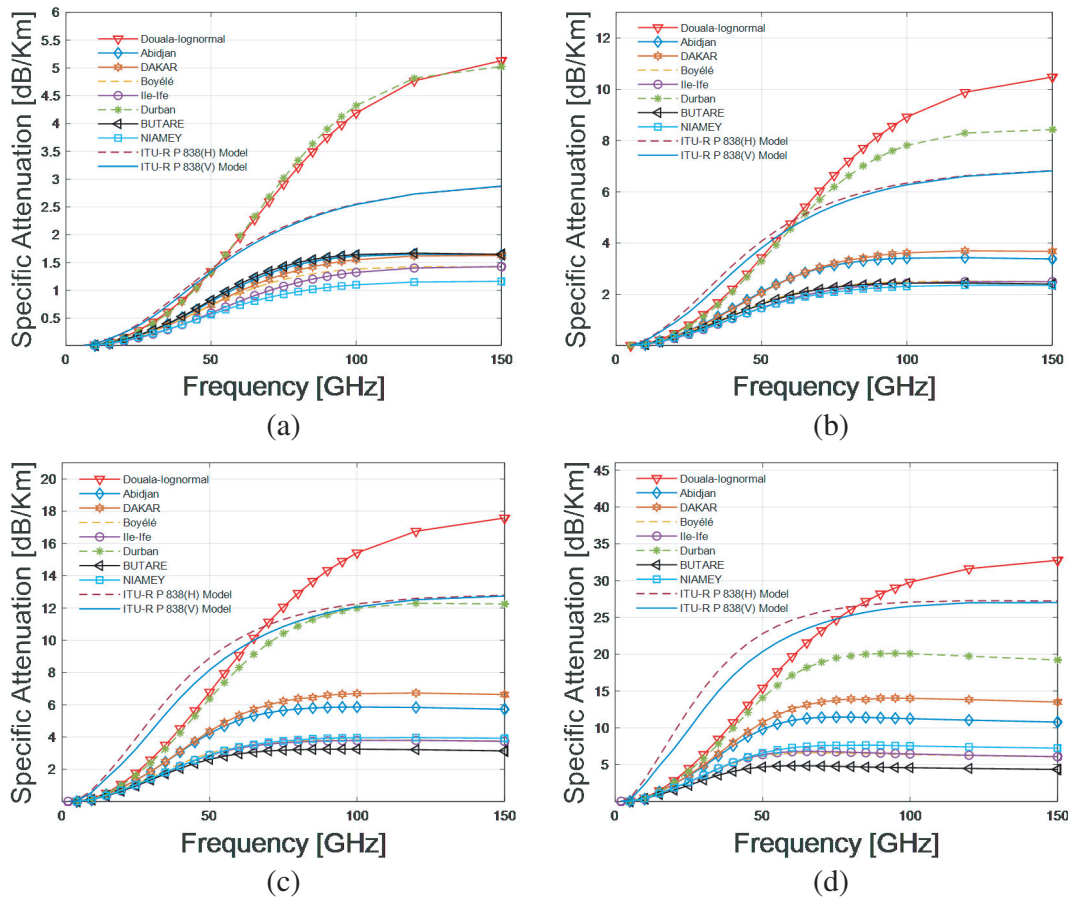
Figure 2. Specific attenuation for lognormal and gamma models with frequency at rain rate (a) 5 mm/h, (b) 10 mm/h, (c) 30 mm/h and (d) 80 mm/h.

attenuation predictions of the proposed DSD models are observed at four rain rates: low at 2.5 mm/h and 9.5 mm/h and high at 25 mm/h and 80 mm/h, respectively.

The resulting plots are shown in Fig. 3(a), at $R = 2.5$ mm/h, for the Durban and Douala $N(D)$ model. It is observed that both of them perform close to the two ITU-R models (horizontal and vertical polarizations) for the frequency range 10–45 GHz. Above 45 GHz, the ITU-R models underestimate the attenuation.

Table 4. Lognormal parameters for Douala, Ile-Ife, Durban, Abidjan, Butare, Niamey, Boyélé and Dakar.

Lognormal Parameter			
Site	N_T (mm^{-1})	D_g (mm)	σ_g (mm)
Douala	$240.97R^{0.543}$	$0.748R^{0.069}$	$1.349R^{0.042}$
Ile-Ife	$108R^{0.363}$	$0.8228R^{0.199}$	$1.4552R^{-0.021}$
Durban	$262.16R^{0.3992}$	$0.731R^{0.1457}$	$1.3028R^{0.016}$
Abidjan	$75.22R^{0.5591}$	$0.9847R^{0.1236}$	$1.3437R^{-0.001}$
Butare	$95.621R^{0.304}$	$0.9416R^{0.184}$	$1.3119R^{0.0122}$
Niamey	$54.897R^{0.5414}$	$0.9437R^{0.1449}$	$1.4928R^{-0.012}$
Boyélé	$73.432R^{0.4379}$	$0.9598R^{0.1646}$	$1.4246R^{-0.009}$
Dakar	$70.69R^{0.6213}$	$0.9474R^{0.1083}$	$1.4145R^{-0.003}$

Figure 3. Comparison of specific attenuation (A (dB/km)) for Douala and selected tropical, subtropical and semi-arid regions of Africa. (a) 2.5 mm/h. (b) 9.5 mm/h. (c) 25 mm/h. (d) 80 mm/h.

In Fig. 3(b), at $R = 9.5$ mm/h, it is observed that the specific attenuation for each of eight sites more or less matches the value predicted by ITU-R in the frequency range 0–10 GHz. It can also be observed that the ITU-R models overestimate the attenuation for frequencies less than 55 GHz for Douala and less than 65 GHz for Durban, while they underestimate beyond those frequencies.

In Fig. 2 and Fig. 3, the increase of frequency and rain rate causes a significant increase in rain attenuation. For a higher rain rate (Fig. 2(d) and Fig. 3(d)), the ITU-R models overestimate the specific attenuation for all sites, except for the Douala site where the underestimation appears for frequencies below 65 GHz (for horizontal polarization) and for frequencies below 55 GHz (for vertical polarization).

The difference observed between the ITU-R model's attenuation values and local DSD generated attenuation values indicates a mismatch between the observed DSD and Laws-Person model of DSD [32]. This is expected since the ITU-R model is developed using data from the temperate region [38, 39], where the rainfall characteristics are different from those in the tropical region.

It can be observed that Douala characterized by equatorial climate and Durban characterized by subtropical climate show similar attenuation characteristics for lower rain rate. The rain attenuation at Douala is always higher than other locations for a higher rain rate. The reason may be that the measured data have a lot of low precipitation (events < 10 mm/h), e.g., for the 10935 spectrum recorded, and 10171 spectrum has a rain rate less than 10 mm/h. These results demonstrate and confirm a strong impact of local climate on the raindrop formation process as well as the relationship with meso-scale weather [32].

4. CONCLUSION

Raindrop size distribution measurements obtained from Douala, Cameroon, a coastal region in Africa, have been analyzed in this study using Parsivel^2 disdrometer data. Two different statistical rainfall DSD models (which are lognormal and gamma models) are examined, and their corresponding input fit parameters are determined using the moment method estimation technique. Error analysis showed that the lognormal model is a slightly better representation of the rainfall DSD in the region than the gamma model. The specific attenuation due to precipitation is estimated, and it increases with increasing frequency and rain rate. The current analysis of the Douala data showed that significant deviations in specific attenuation from the ITUR values could be expected, especially at higher frequencies. At frequencies up to 60 GHz, with lower rain rates, the agreement with the ITUR model is slightly good. At higher frequencies and higher precipitation rates, the attenuations obtained are higher than those predicted by the ITU-R model. The results also showed that, for high frequencies, the gamma model has a higher attenuation value than the lognormal model. The lognormal model is also compared with those of some countries in the tropical, subtropical, and semi-arid regions. For low rain rates, Douala, as a coastal city with an equatorial climate, corresponds most closely to Durban, which has a subtropical climate. This can be justified by the fact that data recorded in Douala contain more events with low-intensity rates. The comparison allowed us to highlight the particularity of the attenuation in the city of Douala. It should be mentioned that the results in this work are a preliminary investigation as the data used are not sufficient to give an affirmative prediction of the attenuation due to rain in this region and on the best choice of the DSD model. The proposed models are very important for the determination of rainfall attenuation for terrestrial and satellite systems.

ACKNOWLEDGMENT

REFERENCES

1. Tridon, F., A. Battaglia, and S. Kneifel, "How to estimate total differential attenuation due to hydrometeors with ground-based multi-frequency radars," 2020.

2. Busari, H. O. and O. A. Fakolujo, "Estimation of attenuation due to rain within Ka and Ku bands in Oyo State of Nigeria," *FUOYE Journal of Engineering and Technology*, Vol. 6, No. 1, 2021.

3. Hong, E. S., S. Lane, D. Murrell, N. Tarasenko, C. Christodoulou, and J. Keeley, "Estimating rain attenuation at 72 and 84 GHz from raindrop size distribution measurements in Albuquerque, NM, USA," *IEEE Geoscience and Remote Sensing Letters*, Vol. 16, No. 8, 1175–1179, 2019.

4. Liao, L., R. Meneghini, T. Iguchi, and A. Tokay, "Characteristics of DSD bulk parameters: Implication for radar rain retrieval," *Atmosphere*, Vol. 11, No. 6, 670, 2020.

5. Tan, Y. H., K. Saito, J. I. Takada, M. R. Islam, and A. R. Tharek, "Rain attenuation prediction based on theoretical method with realistic drop shape for millimeter-wave radio in tropical region," *IEICE Communications Express*, 2021.

6. Sumbiri, D. and T. J. Afullo, "Optimized rain drop size distribution model for microwave propagation for equatorial Africa," *SAIEE Africa Research Journal*, Vol. 111, No. 1, 22–35, 2020.

7. Ojo, J., M. Ajewole, and S. Sarkar, "Rain rate and rain attenuation prediction for satellite communication in Ku and Ka bands over Nigeria," *Progress In Electromagnetics Research B*, Vol. 5, 207–223, 2008.

8. Ochou, A. D., A. Nzeukou, and H. Sauvageot, "Parametrization of drop size distribution with rain rate," *Atmospheric Research*, Vol. 84, No. 1, 58–66, 2007.

9. Alonge, A. A. and T. J. Afullo, "Rainfall microstructures for microwave and millimeter wave link budget at tropical and subtropical sites," *2013 Africon.*, IEEE, 1–5, 2013.

10. Adetan, O., "Preliminary investigation of raindrop size distribution modelling for microwave applications in Rwanda," *IOSR Journal of Engineering*, Vol. 4, No. 7, 01–09, 2013.

11. Ajayi, G. O. and R. L. Olsen, "Modeling of a tropical raindrop size distribution for microwave and millimeter wave applications," *Radio Science*, Vol. 20, No. 02, 193–202, 1985.

12. Battaglia, A., E. Rustemeier, A. Tokay, U. Blahak, and C. Simmer, "PARSIVEL snow observations: A critical assessment," *Journal of Atmospheric and Oceanic Technology*, Vol. 27, No. 2, 333–344, 2010.

13. Gires, A., I. Tchiguirinskaia, and D. Schertzer, "Two months of disdrometer data in the Paris area," *Earth System Science Data*, Vol. 10, No. 2, 941–950, 2018.

14. Tokay, A., D. B. Wolff, and W. A. Petersen, "Evaluation of the new version of the laser-optical disdrometer, OTT Parsivel^2," *Journal of Atmospheric and Oceanic Technology*, Vol. 31, No. 6, 1276–1288, 2014.

15. Kruger, A. and W. F. Krajewski, "Two-dimensional video disdrometer: A description," *Journal of Atmospheric and Oceanic Technology*, Vol. 19, No. 5, 602–617, 2002.

16. Thurai, M. and V. N. Bringi, "Drop axis ratios from a 2D video disdrometer," *Journal of Atmospheric and Oceanic Technology*, Vol. 22, 966–978, 2005.

17. Beard, K. V., "Terminal velocity adjustment for cloud and precipitation drops aloft," *Journal of Atmospheric Sciences*, Vol. 34, No. 8, 1293–1298, 1977.

18. Feingold, G. and Z. Levin, "The lognormal fit to raindrop spectra from frontal convective clouds in Israel," *Journal of Climate and Applied Meteorology*, Vol. 25, No. 10, 1346–1363, 1986.

19. Sauvageot, H. and J. P. Lacaux, "The shape of averaged drop size distributions," *Journal of Atmospheric Sciences*, Vol. 52, No. 8, 1070–1083, 1995.

20. Moumouni, S., M. Gosset, and E. Houngninou, "Main features of rain drop size distributions observed in Benin, West Africa, with optical disdrometers," *Geophysical Research Letters*, Vol. 35, No. 23, 2008.

21. Alonge, A. A., "Semi-empirical characteristics of modified lognormal DSD inputs using rain rate distributions for radio links over the African continent," *Advances in Space Research*, Vol. 67, No. 1, 179–197, 2021.

22. Yakubu, M. L., Z. Yusop, and F. Yusof, "The modelled raindrop size distribution of Skudai, Peninsular Malaysia, using exponential and lognormal distributions," *The Scientific World Journal*, Vol. 2014, 2014.

23. Ulbrich, C. W. and D. Atlas, "Microphysics of raindrop size spectra: Tropical continental and maritime storms," *Journal of Applied Meteorology and Climatology*, Vol. 46, No. 11, 1777–1791, 2007.

24. Zhang, G., J. Vivekanandan, E. A. Brandes, R. Meneghini, and T. Kozu, "The shape-slope relation in observed gamma raindrop size distributions: Statistical error or useful information?," *Journal of Atmospheric and Oceanic Technology*, Vol. 20, No. 8, 1106–1119, 2003.

25. Kozu, T. and K. Nakamura, "Rainfall parameter estimation from dualradar measurements combining reflectivity profile and path-integrated attenuation," *J. Atmos. Ocean. Technol.*, Vol. 8, 259–270, 1991.

26. Afullo, T. J. O., "Raindrop size distribution modeling for radio link design along the eastern coast of South Africa," *Progress In Electromagnetics Research B*, Vol. 34, 345–366, 2011.

27. Shayea, I., T. A. Rahman, M. H. Azmi, and M. R. Islam, "Real measurement study for rain rate and rain attenuation conducted over 26 GHz microwave 5G link system in Malaysia," *IEEE Access*, Vol. 6, 19044–19064, IEEE, 2018.

28. Marzuki, M., T. Kozu, T. Shimomai, W. L. Randeu, H. Hashiguchi, and Y. Shibagaki, "Diurnal variation of rain attenuation obtained from measurement of raindrop size distribution in equatorial Indonesia," *IEEE Transactions on Antennas and Propagation*, Vol. 57, No. 4, 1191–1196, 2009.

29. Lam, H. Y., J. Din, L. Luini, A. D. Panagopoulos, and C. Capsoni, "Analysis of raindrop size distribution characteristics in Malaysia for rain attenuation prediction," *IEEE 2011 XXXth URSI General Assembly and Scientific Symposium*, 1–4, 2011.

30. Maitra, A., "Rain attenuation modeling from measurements of rain drop size distribution in the Indian region," *IEEE Antennas and Wireless Propagation Letters*, Vol. 3, No. 1, 180–181, 2004.

31. Liebe, H. J., G. A. Hufford, and T. Manabe, "A model for the complex permittivity of water at frequencies below 1 THz," *Internat. J. Infrared and mm Waves*, Vol. 12, No. 7, 659–675, 1991.

32. Das, S. and A. Maitra, "Rain attenuation modeling in the 10–100 GHz frequency using drop size distributions for different climatic zones in tropical India," *Progress In Electromagnetics Research B*, Vol. 25, 211–224, 2010.

33. Olsen, R. L., D. V. Rogers, and D. B. Hodge, "The aR^b relation in the calculation of rain attenuation," *IEEE Transactions on Antennas and Propagation*, Vol. 26, No. 2, 547–556, 1978.

34. Adetan, O. and T. J. Afullo, "Raindrop size distribution and rainfall attenuation modeling in equatorial and subtropical Africa: The critical diameters," *Annals of Telecommunications-Annales des Telecommunications*, Vol. 69, No. 11, 607–619, 2014.

35. Mehta, S., S. Singh, A. Mitra, S. K. Ghosh, S. Raha, and S. K. Mehta, "Modeling of raindrop size distribution observed using micro rain radar over Darjeeling (27.05°N, 88.26°E): An Eastern Himalayan Region," *Pure and Applied Geophysics*, Vol. 177, No. 6, 2959–2976, 2020.

36. Coko, D. and I. Marinovic, "Experimental verification of a deterministic UWB channel model for single room propagation scenarios," *International Journal on Communications Antenna and Propagation*, Vol. 4, No. 2, 37–43, 2014.

37. ITU-R, Rec. 838-3, "Specific attenuation model for rain for use in prediction methods," Intern. Telecom. Union, Geneva, 2005.

38. Crane, R. K., *Electromagnetic Wave Propagation through Rain*, 1st Edition, University of Oklahoma, 1996.

39. Ippolito, L. J., *Radio Wave Propagation in Satellite Communications*, 1st Edition, Van Nostrand Reinhold Company, New York, 1986.